4Pi spectral self-interference microscopy

Brynmor J. Davis,[1,*] Mehmet Dogan,[2] Bennett B. Goldberg,[2,3,4] William C. Karl,[3,4] M. Selim Ünlü,[3,4] and Anna K. Swan[3]

[1]*Beckman Institute for Advanced Science and Technology, University of Illinois at Urbana–Champaign, Urbana, Illinois 61801, USA*

[2]*Department of Physics, Boston University, Boston, Massachusetts 02215, USA*

[3]*Department of Electrical and Computer Engineering, Boston University, Boston, Massachusetts 02215, USA*

[4]*Department of Biomedical Engineering, Boston University, Boston, Massachusetts 02215, USA*

**Corresponding author: bryn@uiuc.edu*

Received May 14, 2007; revised October 3, 2007; accepted October 3, 2007; posted October 11, 2007 (Doc. ID 83056); published November 21, 2007

Spectral self-interference microscopy (SSM) relies on the balanced collection of light traveling two different paths from the sample to the detector, one direct and the other indirect from a reflecting substrate. The resulting spectral interference effects allow nanometer-scale axial localization of isolated emitters. To produce spectral fringes the difference between the two optical paths must be significant. Consequently, to ensure that both contributions are in focus, a low-numerical-aperture objective lens must be used, giving poor lateral resolution. Here this limitation is overcome using a 4Pi apparatus to produce the requisite two paths to the detector. The resulting instrument generalizes both SSM and 4Pi microscopy and allows a quantification of SSM resolution (rather than localization precision). Specifically, SSM is shown to be subject to the same resolution constraints as 4Pi microscopy. © 2007 Optical Society of America

OCIS codes: 100.3020, 110.4850, 110.6880, 120.3180, 120.6200, 170.2520.

1. INTRODUCTION

Fluorescence microscopy is a central tool in both the structural and functional study of biological systems. Dyes can be attached with great specificity to structures of interest and the resulting fluorescent emission used for *in vivo* imaging. While fluorescence microscopy is of great utility, it is subject to several well-known limitations. Foremost among these is the diffraction limit [1]. Imaging biological samples nondestructively places a lower limit on the wavelength of the interrogating light and thus limits the resolution accordingly. Much investigative effort has been focused on overcoming the diffraction limit in fluorescence microscopy using a variety of mechanisms. The exploitation of nonlinear optical fluorophore properties has been a particularly successful method [2–5] but generally requires additional instrumentation, measurements, and/or signal processing.

Alternatively, if certain properties of the object are known *a priori*, it may be possible to localize structures with a precision well below the conventional resolution limit. This approach is exemplified in far-field single-molecule microscopy [6], where the object is known to consist of a single pointlike molecule. It has been shown the molecule can be localized using conventional instrumentation to a precision over two orders of magnitude greater than the diffraction-limited resolution [7,8]. At visible wavelengths this localization precision is of the order of a nanometer. High localization precision has allowed single molecule studies to produce significant results in biological research (e.g., [9]). It is important to note that localization and resolution are distinct concepts—the former refers to the precision achievable when estimating the position of a known structure, while the latter gives the minimum scale visible in the estimate of an unknown object distribution.

Spectral self-interference microscopy (SSM) [10–12], like single-molecule microscopy, localizes fluorescent structures by seeking object parameters that minimize the difference between the observed data and those given by a numerical model of the system. SSM also produces nanometer-scale localization and has been used in biological studies [13]. Unlike single-molecule microscopy, which usually localizes fluorophores in the lateral plane (perpendicular to the optic axis of the objective lens), SSM provides localization in the axial direction. Lateral resolution is attained in the traditional manner—by focusing produced by the objective lens.

SSM has both advantages and drawbacks when compared with other three-dimensional fluorescence microscopy instruments. Many instruments, for example confocal microscopes [14], rely on scanning the focus of an objective lens through the sample in three dimensions. This process is typically time-consuming and involves exposing the fluorophores to high doses of excitation light. This can cause the fluorophores to bleach, that is to cease emitting light. SSM does not require axial scanning so the dosage can be substantially reduced. However, traditional SSM requires the use of low-numerical-aperture (NA) lenses, as explained later in this paper. As a result, the lateral resolution is less than can be achieved by high-NA systems. Additionally, low-NA objective lenses subtend only a small range of angles and therefore are inherently limited in their collection efficiency—potentially a major drawback in photon-scarce applications. Traditional SSM also requires the sample to be mounted on a reflecting substrate.

As explained below, SSM bears many similarities to 4Pi microscopy [15,16]. Like SSM, 4Pi microscopes can be used to localize structures axially with nanometer precision [17]. Unlike SSM, this requires axial scanning and therefore may have the associated bleaching problems. 4Pi microscopy does allow the use of high-NA lenses and exhibits the associated high lateral resolution. To date, implementations of SSM have had a low lateral resolution and a low collection efficiency due to the low-NA objective lenses. As a result they have been applied only to axially layered samples, and the resulting axial position estimate is understood to correspond to an average axial position within the focal volume.

This work demonstrates a hybrid SSM–4Pi instrument—a generalization of both systems. In this instrument high-NA objective lenses can be employed with the result that a high lateral resolution can be achieved. Additionally, provided that the structure of interest is within the focal volume, its axial position can be determined with nanometer precision but without the requirement for axial scanning. In this manner the advantages of both SSM and 4Pi are realized. Additionally, the hybrid instrument clarifies the resolution limits, as opposed to the localization precision, of SSM. In other words, the performance of SSM when imaging an arbitrary, unknown object is quantified.

Section 2 gives a brief summary of 4Pi and SSM systems before discussing the hybrid instrument. In Section 3 the point-spread functions (PSFs) and optical-transfer functions (OTFs) of the hybrid 4Pi–SSM system are derived. This gives a characterization of the proposed instrument. Experimental results are given in Section 4 before a closing discussion is given.

2. SPECTRAL SELF-INTERFERENCE AND 4Pi MICROSCOPY

This section gives a brief outline of spectral self-interference microscopy and 4Pi microscopy. The connection between the two is explained and used to define a hybrid instrument.

A. Spectral Self-Interference Microscopy

In SSM the fluorescent object is placed above a reflecting surface, optically excited, and the resulting emitted light is measured spectroscopically. A simple schematic of this is shown in Fig. 1. In addition to the direct optical path from the object to the detector, the mirror produces an additional reflected path. These two routes produce interference in the detected light, and since the fixed physical path corresponds to a wavelength-dependent optical path, each component of the detected spectrum will exhibit a different interference effect. As the detected wavelength changes, the interference cycles between constructive and destructive cases producing oscillations in the spectrum. The period and position of these oscillations depend on the height of the emitter above the mirror, and thus the axial position of the emitter is encoded in the spectrum. The appropriate processing allows the axial position to be recovered from the spectrum.

As shown in Fig. 1, the excitation and detection may be focused. This allows the imaged region to be confined laterally. Lateral scanning of the focal spot will therefore allow a three-dimensional image to be constructed. It should also be noted that because of the lens and mirror, the excitation intensity will not be uniform throughout the sample—it will be focused (to provide lateral resolution) and will also exhibit interference effects.

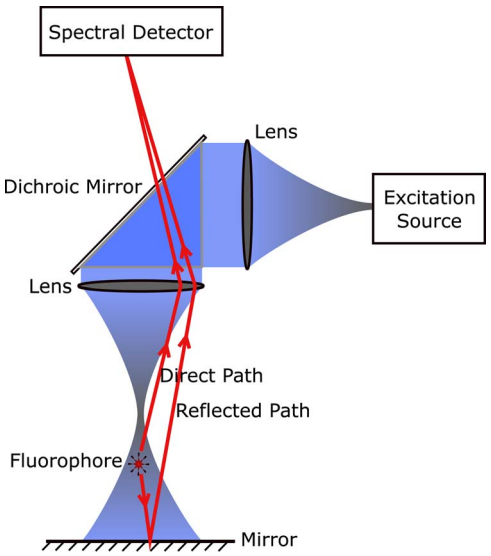

Fig. 1. (Color online) Basic illustration of one implementation of fluorescence spectral self-interference microscopy. Note that the light from the excitation source has been shown as focused while a ray illustration has been used for the emission. This is solely to provide a clear distinction between the two—both excitation and emission light undergo focusing effects.

To achieve oscillations in the measured spectrum, the optical path lengths of the two paths should differ by several multiples of 2π over the emission band of the fluorophore. For typical spectral profiles this necessitates a round-trip path difference of the order of a few tens of wavelengths. As the reflected light traverses this additional distance it will spread, as shown in Fig. 2. To have both the direct and reflected paths in focus at the detector, as required for high-contrast fringes, it is necessary to have an objective lens with a depth of field that exceeds the path difference. This necessitates the use of low-NA lenses, which limits the achievable lateral spot size and the collection efficiency.

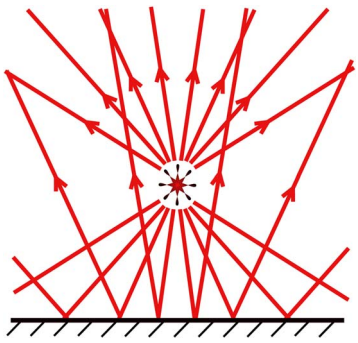

Fig. 2. (Color online) Ray illustration of the difference in focusing between the direct and reflected paths in SSM. The two contributions converge to different points which cannot be simultaneously at the focal point of the objective lens.

B. 4Pi Microscopy

4Pi microscopy is a high-resolution, three-dimensional imaging technique. This method illuminates and detects in a coherent manner from both sides of the object. The resulting interference effects are exploited to give a higher resolution than comparable noninterferometric systems. A basic diagram of a 4Pi system is shown in Fig. 3.

In 4Pi microscopy the foci of the two objective lenses coincide and care is taken to ensure that the optical path lengths in each arm of the interferometer are equal. This ensures that the emission from the fluorophore travels the two paths in equal time and interferes at the detector. Similarly, interference effects are seen in the excitation light. As a result, an axial standing wave structure is seen in the focal volume so that the PSF has a sharp central peak and lower sidelobes. The effect of the sidelobes in the data can be removed by using appropriate deconvolution techniques [18]. As in SSM, inversion processing is required to produce a usable image. However the focal spot must be scanned through three dimensions to construct a three-dimensional image (cf. SSM in which only the two lateral directions need to be scanned). 4Pi microscopy does have the advantage of being able to use high-NA lenses and exhibits the consequent improvements in resolution and collection efficiency.

C. Connecting SSM and 4Pi Microscopy

Although SSM and 4Pi are implemented in very different fashions, they both rely on interference produced by two paths to/from the object. The excitation and collection via the reflections from the SSM mirror are very similar to the action of the second objective path in 4Pi microscopy. The connection between a 4Pi system and a system with a single objective over a mirror (as in SSM) has also been noted in the literature [19]. While the operating principles of 4Pi and SSM are somewhat similar there are several key differences:

1. *Spectral Detection*—SSM relies on spectral detection to determine the axial position of the imaged fluorophore. 4Pi microscopes typically collect light in a window around a single central wavelength. Multiwavelength 4Pi systems have been implemented [20] but their purpose is to simultaneously image a multiply stained object rather than to measure the spectrum from a single dye.
2. *Scanning*—SSM scans in the lateral directions only, as the axial resolution is provided by the spectral self-interference effect. By contrast, 4Pi microscopes scan in all three spatial dimensions when creating a three-dimensional image. However, it should be noted that a thick object may occupy an axial region greater than the depth of focus in SSM. SSM imaging of such an object may require some form of coarse axial scanning.
3. *Unequal Path Lengths*—SSM relies on a difference between the two path lengths to produce wavelength-dependent interference and the characteristic spectral signatures. Equal optical path lengths are usually used in 4Pi microscopy so that both the excitation and detection patterns have a constructive peak at the twin lenses' focal point. 4Pi experiments with destructive interference have been conducted [21], but no resulting advantage was demonstrated. If the path lengths in a 4Pi microscope differ by more than the fluorescent emission coherence length, the spectral fringes will wash out across the wavelengths to which the detector is sensitive, and no interference effects will be observed. Fine spectral resolution is employed in SSM so that the fringes can be seen.
4. *Foci Offset*—The foci of the two objectives are matched in 4Pi microscopy, but this is not possible in SSM. In SSM the two optical paths are of different length, but both pass through the same objective lens. This implies that both paths cannot be simultaneously focused to the same point.
5. *Mirror Effects*—In general, the mirror in SSM will have a reflection coefficient of less than 1 and will introduce a phase shift. This reflection coefficient may also vary with incidence angle and thus modify the angular distribution of the reflected light. By contrast, a 4Pi system will have balanced power in both optical paths and (ideally) be free of phase shifts and angular distortions.

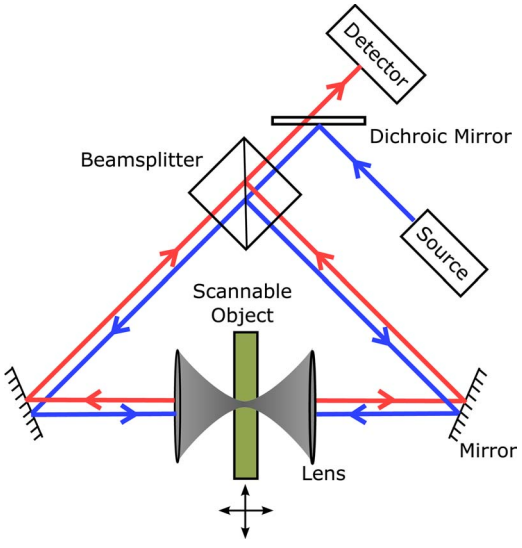

Fig. 3. (Color online) Simplified schematic of a 4Pi Type C microscope. Excitation and detection are both through twin opposing objective lenses.

Considering these differences, it is possible to define a generalized SSM instrument that will include 4Pi operation as a special case. This generalized instrument will be based on a 4Pi microscope but include spectral detection, a user-defined path difference between the two arms, and possibly mismatched foci. Mirror effects will not be included as the ideal SSM system would have a mirror with reflectivity of 1. This would result in balanced power in the two paths (as in 4Pi) and thus maximum contrast in the spectral fringes. Since this hybrid system is a generalization of 4Pi and SSM, its resolution limits are upper bounds for both these methods.

In standard SSM the difference in the path lengths is necessarily associated with an effective offset between the foci of the two paths. This effect is illustrated in Fig. 2. While the path difference is introduced on the sample side of the objective lens in SSM, it can be introduced via a change in interferometer arm length in the 4Pi–SSM instrument. This decouples the foci offset and path length difference. As a result, the path length difference can be

present while maintaining the matched foci of both paths to the detector. As a result, the large depth of field is no longer necessary and high-NA lenses can be used. Further description of 4Pi–SSM instrumentation can be found in Section 4.

3. CHARACTERIZATION OF 4Pi–SSM

A. Point-Spread Function Analysis

A 4Pi microscope has a linear shift-invariant (LSI) relationship between the object and the data collected, and can therefore be described by a PSF $h_{4\mathrm{Pi}}(\mathbf{r})$ [15]. Here $\mathbf{r}=(x,y,z)$ indicates the spatial coordinates, with z quantifying the axial position and x and y being the lateral axes. The generalized SSM system described in the previous section maps a three-dimensional object to a data set with up to four dimensions (three spatial/scanning dimensions and a spectral dimension). If the 4Pi–SSM system scans only in the lateral dimensions, the three-dimensional object will be mapped to two spatial dimensions and a spectral dimension.

To describe this system, consider the data collected at a single wavelength λ_d. The relationship between the object and the data over the remaining three spatial dimensions is linear and shift-invariant. A PSF can therefore be defined for each detection wavelength. This implies the spectral instrument can be regarded as a set of parallel LSI microscopes, each collecting data at a different detection wavelength. Thus the generalized 4Pi–SSM instrument is described by a set of PSFs—one for each detection wavelength.

The 4Pi PSF can be constructed from the focused electric fields produced by the two objective lenses. These vector fields depend on the wavelength considered and will be denoted by $\mathbf{a}_1(\mathbf{r};\lambda)$ and $\mathbf{a}_2(\mathbf{r};\lambda)$. Methods of calculating these fields are well known [22]. If the lenses are well-matched, these two fields will be the same except for opposite propagation directions. The construction of the 4Pi PSF is known [15] to be

$$h_{4\mathrm{Pi}}(\mathbf{r}) = |\mathbf{a}_1(\mathbf{r};\lambda_e) + \mathbf{a}_2(\mathbf{r};\lambda_e)|^2 |\mathbf{a}_1(\mathbf{r};\lambda_d) + \mathbf{a}_2(\mathbf{r};\lambda_d)|^2, \quad (1)$$

where λ_e is the excitation wavelength. The PSF is the product of two intensity distributions—one for the excitation and one for the detection. The two counterpropagating amplitudes add coherently in each, and the square magnitude is taken to get the intensity.

It should be noted that Eq. (1) assumes a linear and isotropic optical response for the fluorophores. Directional object responses can be accounted for by constructing PSFs for different combinations of polarization directions [23], giving an instrument model sensitive to object anisotropy. This technique has been described for fluorescence microscopy [12] but is not employed here. Additionally, Eq. (1) assumes that the detected polarization direction is equal to the polarization of the excitation light before it is focused. This can be easily generalized to cover an arbitrary detection polarization including the case where the detection is not polarization sensitive [12,24]. For simplicity, Eq. (1) will be used with the understanding that the results derived are not limited to this single detection-polarization state.

The PSF for the generalized 4Pi–SSM instrument at a detection wavelength of λ_d will be denoted by $h_{4\mathrm{Pi-SSM}}(\mathbf{r};\lambda_d)$. This can be constructed in the same fashion as the 4Pi PSF but with some adjustments to account for the system modifications described in Subsection 2.C. The spectral detection is implicitly modeled by the fact that the PSF is parameterized by λ_d; that is, there is a different PSF at each detection wavelength. The path length difference between the two arms will introduce a phase delay ϕ between the two focused fields. In the excitation fields, this delay ϕ_e will be constant as the excitation wavelength is not varied. However, in the detection field ϕ_d will depend on the wavelength λ_d, as the optical path difference changes with wavelength. If the difference in the free-space path lengths is D, then the difference in optical path is characterized by the phase

$$\phi_d(\lambda_d) = \frac{2\pi D}{\lambda_d}. \quad (2)$$

This dependence is what produces the spectral oscillations in SSM.

The offset between foci results in an offset $\mathbf{r}_o$ between the focused fields. Without loss of generality, the path difference and foci offset can be included in the second focused field. The resulting change in $\mathbf{a}_2(\mathbf{r};\lambda)$ between the 4Pi and 4Pi–SSM cases is

$$\mathbf{a}_2(\mathbf{r};\lambda) \Rightarrow e^{i\phi(\lambda)}\mathbf{a}_2(\mathbf{r}-\mathbf{r}_o;\lambda). \quad (3)$$

Substituting into Eq. (1) results in the following expression for the PSFs of the 4Pi–SSM system:

$$h_{4\mathrm{Pi-SSM}}(\mathbf{r};\lambda_d) = |\mathbf{a}_1(\mathbf{r};\lambda_e) + e^{i\phi_e}\mathbf{a}_2(\mathbf{r}-\mathbf{r}_o;\lambda_e)|^2 \times |\mathbf{a}_1(\mathbf{r};\lambda_d) + e^{i\phi_d(\lambda_d)}\mathbf{a}_2(\mathbf{r}-\mathbf{r}_o;\lambda_d)|^2. \quad (4)$$

It is clear that 4Pi operation can be achieved using the 4Pi–SSM system described, for if $\mathbf{r}_o=\mathbf{0}$ and $\phi_e=\phi_d(\lambda_d)=0$ then Eq. (4) becomes Eq. (1).

Using Eq. (4), example 4Pi–SSM PSFs can be calculated. An excitation wavelength of 488 nm is used and the fluorophore is assumed to emit between 510 and 590 nm. The objective lenses have a numerical aperture of 1.4 and operate in a medium with a refractive index of 1.518. Excitation light linearly polarized in the x direction is used and the detector is assumed insensitive to polarization state. The example PSFs can be seen in Fig. 4.

Each of the PSFs in Fig. 4 characterizes the SSM imaging for a given detection wavelength, foci offset, and pair of phases. The smaller the structure in the PSF, the greater the attainable resolution will be. Consequently the PSFs for $\lambda_d=510$ nm can be expected to provide slightly better resolution. However, differences between the $\lambda_d=510$ and $\lambda_d=590$ nm cases do not appear large in Fig. 4. The PSFs can be seen to be strongly dependent on the phases ϕ_e and ϕ_d. These changes are what result in the spectral fringes seen in SSM. As mentioned earlier, the potential of changing ϕ in a 4Pi system has been explored in the literature [21] but was shown not to provide additional resolution. The effects of ϕ_e and ϕ_d on resolution will be further discussed in Subsection 3.B.

As would be expected, a nonzero foci offset broadens the PSF so that it encompasses both focal points. In addi-

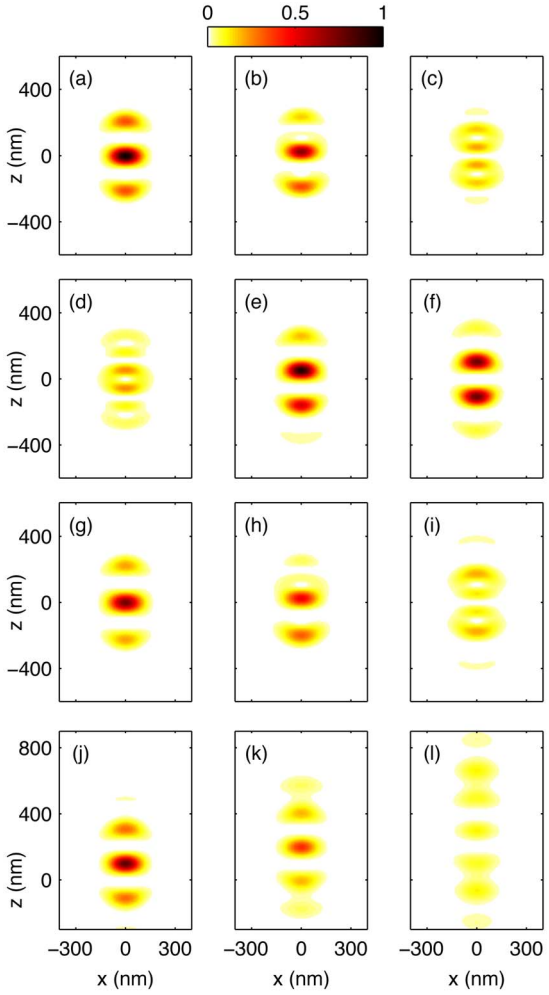

Fig. 4. (Color online) Example point spread functions for a 4Pi–SSM system. These plots are two-dimensional slices (the xz plane) of three-dimensional functions. Instrument parameters that are constant for all plots include NA=1.4, n=1.518, λ_e =488 nm, and the excitation polarization state, before focusing, which is in the x direction. In (a)–(f), λ_d=510 nm and $\mathbf{r}_o=\mathbf{0}$, while (ϕ_e,ϕ_d) is $(0,0)$, $(0,\pi/2)$, $(0,\pi)$, $(\pi,0)$, $(\pi/2,\pi/2)$, and (π,π), respectively. In (g)–(i), λ_d=590 nm and $\mathbf{r}_o=\mathbf{0}$, while (ϕ_e,ϕ_d) is $(0,0)$, $(0,\pi/2)$, and $(0,\pi)$, respectively. In (j)–(l), λ_d=510 nm, and (ϕ_e,ϕ_d)=$(0,0)$, while $\mathbf{r}_o$ is $(0,0,200)$nm, $(0,0,400)$nm, and $(0,0,600)$nm, respectively. A nonlinear display scale is used so that low-level detail is visible.

tion, the overall level of the PSF is lowered, indicating the collection of fewer photons. The largest offset seen in Fig. 4 is 600 nm, while approximately ten micrometers of offset would be required to make the phase [see Eq. (2)] oscillate several times within the given spectral bounds. Increasing the offset to this scale results in a PSF of low magnitude. This indicates that with the high-NA lenses used in this example, having significantly offset foci is not a viable option. The traditional implementation of SSM would not be workable, as both the direct and reflected paths cannot be simultaneously in focus while maintaining a sufficiently large path difference. The 4Pi–SSM system is necessary with high-NA lenses, as the path difference can be substantial without having offset foci.

B. Optical-Transfer Function Analysis

The OTF is the Fourier transform of the PSF and is a powerful tool, as it shows how strongly each spatial frequency is passed by the instrument. The larger the bandwidth displayed by the OTF, the higher the resolution of the microscope. In this section the 4Pi–SSM OTFs are used to quantify the instrument's resolution. It should again be emphasized that resolution is a concept distinct from the localization precision. The OTFs corresponding to the PSFs of Fig. 4 are shown in Fig. 5.

The better OTFs are those that have values significantly greater than zero over the largest range of spatial frequencies. The OTF corresponding to a 510 nm-detection 4Pi instrument is shown in the upper left of Fig. 5. It is arguable that none of the other OTFs have a better profile than this one. The effect of the nonzero phase values has been detrimental at many spatial frequencies in that the OTF values have been lowered. If the OTF value for a given spatial frequency falls below the noise level, it becomes difficult to reconstruct that Fourier component of the image. As a result, resolution suffers. The detrimental effect of the foci offset is also clear in the OTF plots, as significant regions of the OTF have been reduced to a very low level. When comparing 4Pi and 4Pi–SSM systems, these OTFs indicate that the generalization to 4Pi–SSM operation does not improve the resolution of the 4Pi instrument.

The PSFs and OTFs of Fig. 4 and Fig. 5, respectively, indicate that the maximum 4Pi–SSM resolution is similar

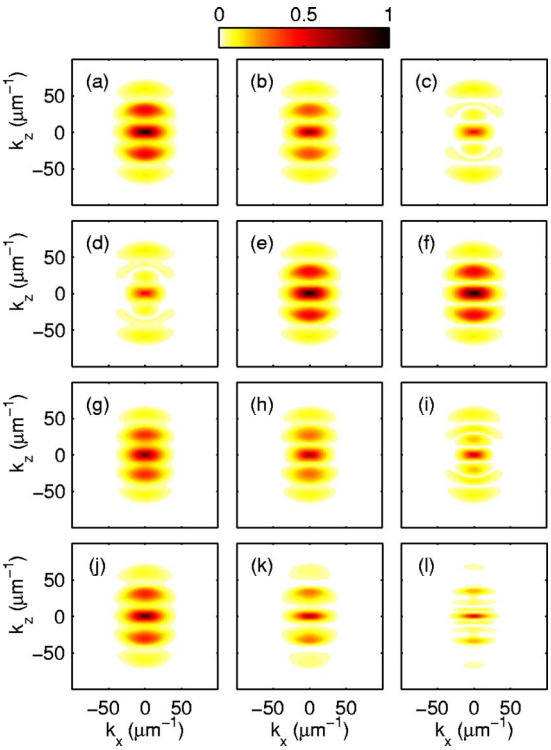

Fig. 5. (Color online) Magnitudes of the OTFs corresponding to the PSFs of Fig. 4. The k_x-k_z plane is shown for each, and the plots have all been scaled by the same constant so that the largest value seen is 1. A nonlinear display scale is used so that low-level detail is visible.

to 4Pi resolution as just noted. This conclusion, though drawn from a single example, is true in general. This can be seen by considering the support of the instrument OTF; i.e., the volume over which the OTF is nonzero. It is possible to prove mathematically that any SSM system will have an OTF support that does not exceed that of a comparable 4Pi system.

The OTF supports of a wide range of far-field focusing microscopes are strictly limited and have been calculated for many systems [25–27]. Finding these supports starts with defining an analytical expression for the OTF [28]. Such an expression has been found for 4Pi systems [29] by taking the Fourier transform of Eq. (1):

$$H_{4\mathrm{Pi}}(\mathbf{k}) = \{[\mathbf{A}_1(\mathbf{k};\lambda_e) + \mathbf{A}_2(\mathbf{k};\lambda_e)] \star [\mathbf{A}_1(\mathbf{k};\lambda_e) + \mathbf{A}_2(\mathbf{k};\lambda_e)]\} * \{[\mathbf{A}_1(\mathbf{k};\lambda_d) + \mathbf{A}_2(\mathbf{k};\lambda_d)] \star [\mathbf{A}_1(\mathbf{k};\lambda_d) + \mathbf{A}_2(\mathbf{k};\lambda_d)]\}. \quad (5)$$

Here $\mathbf{A}(\mathbf{k};\lambda)$ is the spatial Fourier transform of $\mathbf{a}(\mathbf{r};\lambda)$, $*$ is the three-dimensional convolution operator, and $\star$ is the three-dimensional cross-correlation operator.

The function $\mathbf{A}(\mathbf{k};\lambda)$ is used in the calculation of focused vector fields [22] and has been discussed explicitly by McCutchen [30,31]. It is the structure of $\mathbf{A}(\mathbf{k};\lambda)$ that results in the strictly limited support for the microscope OTF. Specifically, $\mathbf{A}(\mathbf{k};\lambda)$ is nonzero only above a certain latitude (defined by the maximum collection angle of the lens) on a spherical surface. Due to the form of the OTF equation [e.g. Eq. (5) for a 4Pi system] the support of the microscope OTF depends only on the support of $\mathbf{A}(\mathbf{k};\lambda)$. Example supports for 4Pi and wide-field systems are shown in Fig. 6. The procedure for calculating the OTF support of a far-field focusing microscope is discussed in [32].

From Fig. 6 it can be seen that 4Pi systems have a significantly larger support, which is consistent with the superior 4Pi resolution. The "missing cone" of axial spatial frequencies is clearly visible in the wide-field support and is known to result in difficulties imaging axial structure in the object [33]. It can also be seen from Figs. 6(b) and 6(c) that a high NA is necessary to create a continuous support in 4Pi systems. Discontinuities in the OTF support can lead to significant artifacts and ambiguities in the final image [34]. Even with a continuous OTF support, noise can limit the range of visible spatial frequencies [35]. As evidenced by comparing Figs. 5(a) and 6(b), the OTF may have very low values within the theoretical support, and these areas may be under the noise floor of the system. This problem has only recently been overcome in single-photon 4Pi systems [36].

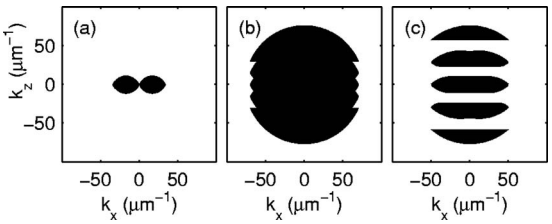

Fig. 6. OTF supports for microscopes with $\lambda_e = 488$ nm, $\lambda_d = 510$ nm, $n = 1.518$. Only the k_x-k_z plane is shown but the support is rotationally symmetric about the k_z axis. The OTF support for a wide-field microscope with a NA of 1.4 is shown in (a). The OTF supports for 4Pi microscopes with NA = 1.4 and NA = 1 are shown in (b) and (c), respectively.

Finding an expression for the 4Pi–SSM OTF also allows its support to be found. The modifications modeled in Eq. (3) can be described in the Fourier domain by

$$\mathbf{A}_2(\mathbf{k};\lambda) \Rightarrow e^{-i[\mathbf{k}\cdot\mathbf{r}_o - \phi(\lambda)]}\mathbf{A}_2(\mathbf{k};\lambda). \quad (6)$$

The 4Pi–SSM OTF is calculated by simply substituting this change into Eq. (5).

It has been shown that a wide range of system modifications do not increase the OTF support of a far-field focusing system [32]. This is also the case here as can be seen from Eq. (6). The effect of the modifications has been simply to multiply $\mathbf{A}_2(\mathbf{k};\lambda)$ by a complex exponential. This does not extend its support and as a result does not extend the support of the 4Pi–SSM OTF. The SSM support changes slightly with detection wavelength but is the same as that of a 4Pi microscope operating at the same wavelength.

Since the spectral self-interference modifications described in Subsection 2.C do not extend the support of the OTF, they do not allow previously unmeasured spatial frequencies to be imaged. This in turn implies that the resolution limits of the system are not increased. While the OTF support cannot be extended, there is a possibility that the OTF values within the support can be raised with respect to the noise level. This sort of imaging improvement has been termed "ultraresolution" [37], as opposed to superresolution which is taken to imply an extension of the OTF support. As seen in Fig. 5, the addition of the phase offsets corresponding to the unequal path lengths does not appear to significantly raise the OTF within the support.

The OTF analysis presented here shows that the 4Pi–SSM instrument has a resolution subject to the same limits as 4Pi microscopy. Additionally, since 4Pi–SSM is a generalization of SSM, the resolution of SSM cannot exceed that of 4Pi microscopy. Nanometer-scale axial localization with high lateral resolution can be achieved in 4Pi microscopy [17] but requires axial scanning through the object. As will be seen in Section 4, 4Pi–SSM removes the requirement for axial scanning. This reduces image acquisition time and also minimizes fluorophore bleaching effects.

4. INSTRUMENT DEMONSTRATION

A prototype 4Pi–SSM has been constructed [38] and is shown in Fig. 7. The instrument is based on a 4Pi Type C confocal microscope in a triangular configuration similar to the one illustrated in Fig. 3. To achieve SSM functionality, the 4Pi microscope is integrated with a spectroscopic detector. The path lengths of the interference arms are adjusted by mounting one of the mirrors on a piezoelectric controller, so that a path difference of several tens of micrometers can be attained. As a result, spectral interference effects can be induced, controlled, and measured.

The excitation source is an optically pumped, semiconductor, continuous-wave laser (Coherent) operating at 488 nm. The laser beam is linearly polarized in the x direction, which is parallel to the beam splitter plane. In or-

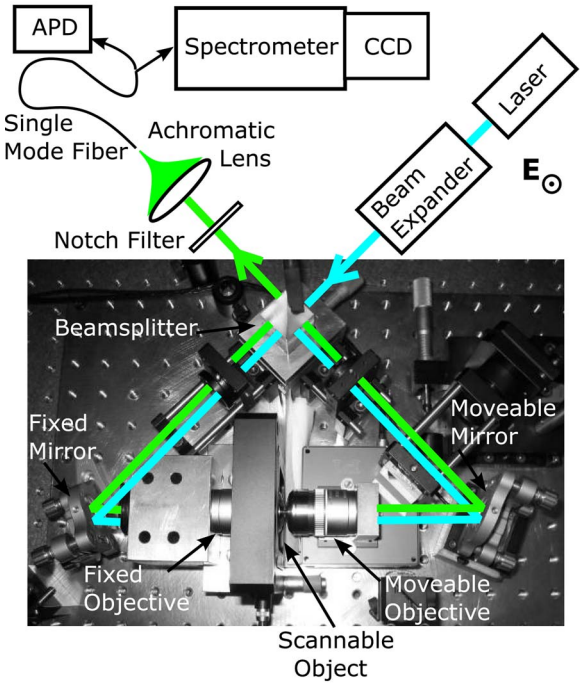

Fig. 7. (Color online) Diagram representing the experimental 4Pi–SSM system used. Beam paths are overlaid on a photograph of the triangular 4Pi microscope unit. The excitation and detection instrumentation are represented schematically, and the polarization of the excitation laser is indicated by **E**. Note that the photograph contains some optical elements not relevant to the discussion presented here—specifically, the mirror with mount behind the text "Moveable Mirror" and the filter cube behind the text "Moveable Objective."

der to achieve a uniform intensity profile at the back aperture of the objectives, the laser beam is expanded with a beam expander so that the beam diameter is about five times that of the back aperture of the objectives.

Two Leica oil-immersion objectives with NA of 1.4 are used to focus the excitation and collect the emission. One of the objectives is mounted on a fixed holder and the second objective is controlled with a piezoelectric stage (Physik Instrumente) in closed loop, allowing nanometer-precision control of the focal position. The objective foci were adjusted to be co-located.

Confocal detection is accomplished using a single-mode fiber as the confocal pinhole. The fiber has a 4.2 μm mode-field diameter and an effective NA of 0.074 at a wavelength of 488 nm. After passing a notch filter for excitation light rejection, the fluorescent signal is focused to the fiber using an achromatic lens with a focal length of 30 mm. For three-dimensional scanning purposes, the collected signal is coupled to an avalanche photodiode (EG&G). During the spectral acquisition, the single-mode fiber is coupled to a spectrometer system that is composed of an f/4 imaging spectrometer (Acton Research) and a CCD camera (Princeton Instruments). The spectral resolution of this spectroscopy system is 45 pm. To eliminate the dark counts of the spectroscopic CCD camera, a background signal was collected with the camera shutter closed before data acquisition. During the spectral measurements, this premeasured background was subtracted online.

As a proof of concept, this microscopy system was used to image two test objects. The first was fluorescent polystyrene beads. These yellow-green, carboxyl-modified FluoSpheres beads from Molecular Probes were specified with 100 nm diameter and excitation/emission maxima of 505/515 nm. The beads were mounted to amine-modified glass coverslip surfaces where 3-aminopropyltriethoxylsilane (APTES) was used for the amine functionalization of the surface. After mounting the beads, immersion oil was applied to the surface, and a second coverslip placed on top and sealed with nail polish. The sample was placed between the two objectives. An image of a bead was acquired by scanning the sample stage (Physik Instrumente) in three dimensions with 20 nm steps. To collect a significant three-dimensional signal, the path length difference was set to zero (so that $\phi_e = \phi_d(\lambda_d) = 0$) and the emissions collected over the full spectral band of the avalanche photodiode. This operation modality corresponds to conventional 4Pi microscopy. A subset of the data collected from a bead is shown in Fig. 8 and compared with theoretical predictions. It can be seen that the observed data are similar to those predicted theoretically.

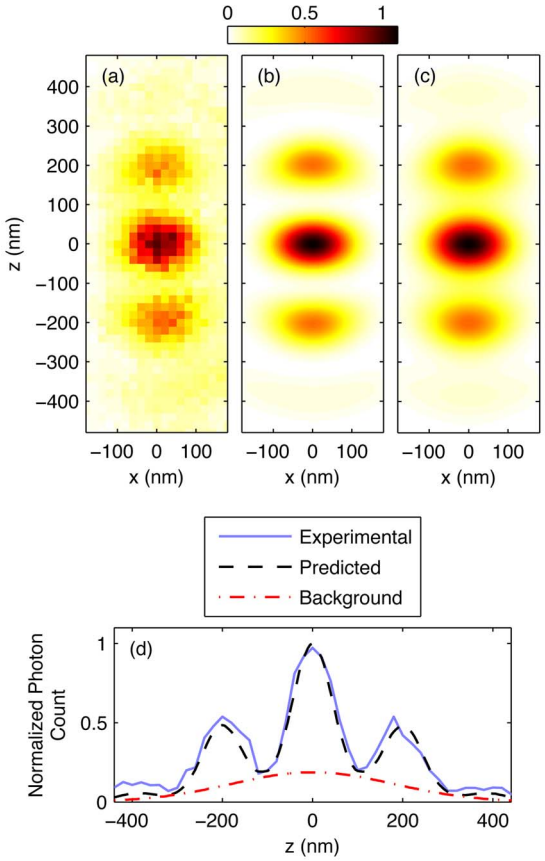

Fig. 8. (Color online) *xz* slice of the data collected by the 4Pi–SSM instrument operating in 4Pi mode from (a) a fluorescent bead, (b) the theoretically predicted data with no background, and (c) the data predicted when the background is modeled. The background model consists of a three-dimensional Gaussian with a standard deviation of 80 nm laterally and 180 nm axially. Axial cross sections of the data, the predicted data (with background included), and the background are given in (d). The spectral envelope $s(\lambda_d)$ used in the model was assumed to be Gaussian and centered around $\lambda_d = 550$ nm with a standard deviation of 25 nm.

Imaging this sort of small object allows the verification of a confined PSF and confirms that the predicted high lateral resolution is achieved. The data collected can be expressed mathematically as

$$f(\mathbf{r}) = \int s(\lambda_d)[h_{4\text{Pi–SSM}}(\mathbf{r};\lambda_d) * o(\mathbf{r})]\mathrm{d}\lambda_d + b(\mathbf{r}), \qquad (7)$$

where $s(\lambda_d)$ is the spectral emission profile of the fluorophore, $o(\mathbf{r})$ is the spatial profile of the bead, and $b(\mathbf{r})$ is a background term. The background term is used to model light that reaches the detector incoherently, e.g., through scattering. Such light does not produce interference at the detector and reduces the contrast of the observed interference fringes. The collection of light through the single-mode fiber also has an effect on the 4Pi–SSM PSF. To model this the Gaussian fiber mode can be projected through the system onto the pupil of the objective lens. This amplitude profile can then be included as an apodization function across the lens. The resulting calculation yields a result consistent with a small loss of NA in the detection optics.

The second object imaged was a lateral layer of Alexa Fluor 488 dye (Invitrogen) deposited on glass coverslips. The Alexa Fluor 488 dye has an absorption/emission maxima of 495/519 nm. This dye also had carboxyl functional groups in order to bind to amine-modified surfaces. The carboxyl-modified Alexa Fluor 488 dye was dissolved in anhydrous dimethyl sulfoxide and incubated on APTES-treated coverslips for 1/2 h. After washing three times with methanol, the surface was dried and another coverslip placed on top with immersion oil between.

This object provides a confined axial structure that can be repeatedly imaged by shifting the focal region across the lateral plane. This has the advantage of allowing the collection of data as a function of both the axial scan position and the detection wavelength without being limited by photobleaching. When a flat thin layer with uniform density is imaged, the data collected are then

$$f(z,\lambda_d) = s(\lambda_d)\left[\int\int h_{4\text{Pi–SSM}}(x,y,z;\lambda_d)\mathrm{d}x\mathrm{d}y + b(z)\right]. \qquad (8)$$

This expression is the convolution of the PSF with the assumed object structure and with a background term $b(z)$ included.

The data collected from the fluorescent layer and predicted data $f(z,\lambda_d)$ are shown in Fig. 9. Again, a strong agreement can be seen. To calculate the predicted data it is necessary to estimate several parameters of the system. The path difference between the two interferometer arms can be found by examining the period of the spectral oscillations. As seen in Eq. (2), a larger difference D results in more rapid oscillations with wavelength. To account for interferometer asymmetries, a detection phase offset $\phi_{d,0}$ is included, so that $\phi_d(\lambda_d) = 2\pi D/\lambda_d + \phi_{d,0}$. The position of the spatial lobes in the data allows the phase ϕ_e to be determined. The parameters D, $\phi_{d,0}$ and ϕ_e, combined with the amplitude and standard deviation of the Gaussian background term, completely define the 4Pi–SSM model. These five parameters were perturbed manually until the fit seen in Fig. 9 was found. As described in [10], the envelope $s(\lambda_d)$ can be found by dividing the measured data by the predicted data and fitting a polynomial to the resulting spectral profile.

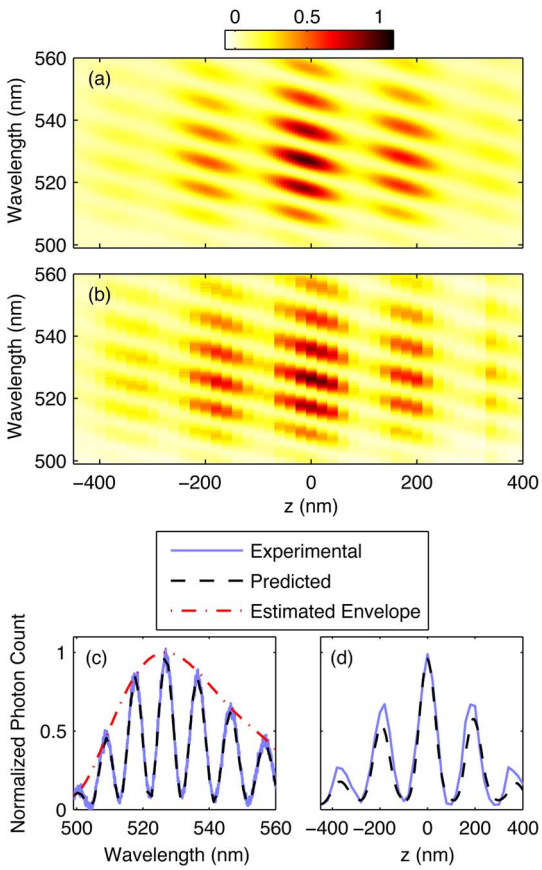

Fig. 9. (Color online) (a) Predicted and (b) measured axial-spectral data from a 4Pi–SSM system when imaging a thin lateral fluorescent layer. The data model is defined by the parameters $D = 29.2\,\mu\text{m}$, $\phi_{d,0} = -0.94\pi$ and $\phi_e = -0.25\pi$. The background term $b(z)$ is Gaussian with an amplitude of 0.06 and a standard deviation of 250 nm. Spectral profiles at $z = 0$ and the estimated spectral envelope $s(\lambda_d)$ are shown in (c), as is a spatial profile at $\lambda_d = 527$ nm in (d).

The data shown in Fig. 9 have features indicative of both 4Pi microscopy and SSM. With the wavelength held fixed, the z profile has the characteristics of the 4Pi PSF. As previously mentioned, nanometer-scale precision can be achieved using nonspectral measurements (4Pi operation) but requires axial scanning to collect a z profile that can be fitted to the expected PSF. If z is held fixed in $f(z,\lambda_d)$, then the spectral profile corresponds to the spectrum observed in SSM when the fluorophore layer is at position z. As can be seen from Fig. 9, the spectral profile changes significantly as z changes. It is this spectral sensitivity that gives SSM the ability to localize structures from a single spectral measurement. That is, given spectral data from a single spatial point, the precise axial position of an emitter (within the focal volume) can be estimated—no axial scanning is required. In the 4Pi–SSM instrument a much smaller lateral area contributes to the signal than in standard SSM and thus the lateral resolution is improved.

As the z position of the object is scanned, the primary change in the spectral profiles seen in Fig. 9 is that the

fringe positions shift. However, over larger ranges of z the period of the oscillations changes significantly. In other words, both the phase and period of the spectral oscillations vary with the position of the object, but the phase varies more rapidly. The period variation has also been exploited in fluorescence coherence tomography [39,40] (FCT), a technique similar to 4Pi–SSM. FCT uses lower-NA lenses and wide-field illumination to produce a microscope completely free of mechanical scanning. Due to the slower variation of the fringe period, FCT produces a much coarser axial profile (with resolution of the order of a few micrometers) but is suitable for the imaging of an arbitrary object. FCT uses coherence imaging analogous to optical coherence tomography to provide axial resolution, as opposed to 4Pi microscopy where the limited axial extent of the focused field is employed. Because of the low-NA lenses used, the lateral resolution in FCT is also much lower than in 4Pi or 4Pi–SSM systems.

The 4Pi–SSM instrument proposed differs from both FCT and 4Pi microscopy in that it provides high-precision information in all three dimensions without the need for axial scanning, and in that it is designed to localize a single structure, not image a general object. It should also be noted that data fitting techniques, as used in the SSM reconstruction algorithm, have been shown to permit the distinction of two closely spaced structures below the traditional resolution limit [41]. SSM can also be used for two-structure imaging [12], but the precision decreases rapidly when more than two object structures are considered.

5. CONCLUSIONS

4Pi–SSM has been described and demonstrated. This technique exploits the commonalities between 4Pi microscopy and spectral self-interference microscopy and generalizes both technologies. The 4Pi–SSM instrument can be mathematically characterized by a set of point-spread functions or optical-transfer functions. This standard mathematical framework allows a comparison between SSM and other microscopy modalities. For example, in this work the PSF/OTF analysis was used to show that SSM is subject to the same resolution limits as 4Pi microscopy.

Through the SSM mechanism, the 4Pi–SSM system allows nanometer-precision axial localization of structures within the focal volume of the cofocused lenses. Like 4Pi microscopy, the contributing lateral range is of the order of a few hundred nanometers. This high lateral resolution is a result of the high-NA lenses that can now be employed, unlike traditional SSM where low-NA lenses are required. The object need not be axially scanned to provide this localization, which provides a significant advantage over 4Pi microscopy. Additionally, 4Pi–SSM does not require the object to be mounted above a reflecting substrate.

It should also be emphasized that if a high lateral resolution is not required, traditional SSM provides a simpler implementation than 4Pi–SSM. The latter is a spectral interferometer and is thus susceptible to alignment and dispersion issues. Small nonidealities may produce artifacts in the image, as has been seen in 4Pi microscopy studies. However, these artifacts may be corrected either in hardware [42,43] or processing [44].

ACKNOWLEDGMENTS

This work was supported in part by the National Science Foundation (grant DBI 0138425 and award EEC-9987821 of the Engineering Research Centers Program), the Air Force Office of Scientific Research (grant MURI F-49620-03-1-0379 and grant FA9550-07-1-0295 to W.C.K.), and the National Institutes of Health (National Institute of Biomedical Imaging and BioEngineering grant 5R01 EB00 756-03). B. J. D. would like to thank P. Scott Carney for comments that helped improve the manuscript and for continuing support of this research.

REFERENCES

1. E. Abbe, "Beiträge zur Theorie des Mikroskops und der Mikroskopischen Wahrnehmung," Arch. Mikrosc. Anat. Entwicklungsmech. **9**, 413–468 (1873).
2. T. A. Klar and S. W. Hell, "Subdiffraction resolution in far-field fluorescence microscopy," Opt. Lett. **24**, 954–956 (1999).
3. R. Heintzmann and T. M. Jovin, "Saturated patterned excitation microscopy—a concept for optical resolution improvement," J. Opt. Soc. Am. A **19**, 1599–1609 (2002).
4. M. G. L. Gustafsson, "Nonlinear structured-illumination microscopy: Wide-field fluorescence imaging with theoretically unlimited resolution," Proc. Natl. Acad. Sci. U.S.A. **102**, 13081–13086 (2005).
5. K. I. Willig, S. O. Rizzoli, V. Westphal, R. Jahn, and S. W. Hell, "STED microscopy reveals that synaptotagmin remains clustered after synaptic vesicle exocytosis," Nature (London) **440**, 935–939 (2006).
6. T. Basché, W. E. Moerner, M. Orrit, and U. P. Wild, eds., *Single-Molecule Optical Detection, Imaging and Spectroscopy* (VCH, 1997).
7. R. J. Ober, S. Ram, and E. S. Ward, "Localization accuracy in single-molecule microscopy," Biophys. J. **86**, 1185–1200 (2004).
8. S. Ram, E. S. Ward, and R. J. Ober, "A stochastic analysis of performance limits for optical microscopes," Multidimens. Syst. Signal Process. **17**, 27–57 (2006).
9. A. Yildiz, J. N. Forkey, S. A. McKinney, T. Ha, Y. E. Goldman, and P. R. Selvin, "Myosin V walks hand-over-hand: Single fluorophore imaging with 1.5-nm localization," Science **300**, 2061–2065 (2003).
10. A. K. Swan, L. A. Moiseev, C. R. Cantor, B. J. Davis, S. B. Ippolito, W. C. Karl, B. B. Goldberg, and M. S. Ünlü, "Toward nanometer-scale resolution in fluorescence microscopy using spectral self-interference," IEEE J. Sel. Top. Quantum Electron. **9**, 294–300 (2003).
11. L. Moiseev, C. R. Cantor, M. I. Aksun, M. Dogan, B. B. Goldberg, A. K. Swan, and M. S. Ünlü, "Spectral self-interference fluorescence microscopy," J. Appl. Phys. **96**, 5311–5315 (2004).
12. B. J. Davis, A. K. Swan, M. S. Ünlü, W. C. Karl, B. B. Goldberg, J. C. Schotland, and P. S. Carney, "Spectral self-interference microscopy for low-signal nanoscale axial imaging," J. Opt. Soc. Am. A **24**, 3587–3599 (2007).
13. L. Moiseev, M. S. Ünlü, A. K. Swan, B. B. Goldberg, and C. R. Cantor, "DNA conformation on surfaces measured by fluorescence self-interference," Proc. Natl. Acad. Sci. U.S.A. **103**, 2623–2628 (2006).
14. T. Wilson and C. J. R. Sheppard, *Theory and Practice of Scanning Optical Microscopy* (Academic, 1984).
15. S. Hell and E. H. K. Stelzer, "Properties of a 4Pi confocal fluorescence microscope," J. Opt. Soc. Am. A **9**, 2159–2166 (1992).
16. S. W. Hell, "Double-scanning microscope," European patent 0491289, 18 December 1990.

17. M. Schmidt, M. Nagorni, and S. W. Hell, "Subresolution axial distance measurements in far-field fluorescence microscopy with precision of 1 nanometer," Rev. Sci. Instrum. **71**, 2742–2745 (2000).
18. M. Schrader, S. W. Hell, and H. T. M. van der Voort, "Three-dimensional super-resolution with a 4Pi-confocal microscope using image restoration," J. Appl. Phys. **84**, 4033–4042 (1998).
19. A. S. van de Nes, L. Billy, S. F. Pereira, and J. J. M. Braat, "Calculation of the vectorial field distribution in a stratified focal region of a high numerical aperture imaging system," Opt. Express **12**, 1281–1293 (2004).
20. H. Kano, S. Jakobs, M. Nagorni, and S. W. Hell, "Dual-color 4Pi-confocal microscopy with 3D-resolution in the 100 nm range," Ultramicroscopy **90**, 207–213 (2002).
21. S. W. Hell and M. Nagorni, "4Pi confocal microscopy with alternate interference," Opt. Lett. **23**, 1567–1569 (1998).
22. B. Richards and E. Wolf, "Electromagnetic diffraction in optical systems. II. Structure of the image field in an aplanatic system," Proc. R. Soc. London, Ser. A **253**, 358–379 (1959).
23. M. R. Arnison and C. J. R. Sheppard, "A 3D vectorial optical transfer function suitable for arbitrary pupil functions," Opt. Commun. **211**, 53–63 (2002).
24. M. Nagorni and S. W. Hell, "Coherent use of opposing lenses for axial resolution increase in fluorescence microscopy. I. Comparative study of concepts," J. Opt. Soc. Am. A **18**, 36–48 (2001).
25. C. J. R. Sheppard, "The spatial frequency cut-off in three-dimensional imaging," Optik (Stuttgart) **72**, 131–133 (1986).
26. C. J. R. Sheppard, "The spatial frequency cut-off in three-dimensional imaging II," Optik (Stuttgart) **74**, 128–129 (1986).
27. M. G. L. Gustafsson, "Extended resolution fluorescence microscopy," Curr. Opin. Struct. Biol. **9**, 627–634 (1999).
28. C. J. R. Sheppard and M. Gu, "Three-dimensional transfer functions for high-aperture systems," J. Opt. Soc. Am. A **11**, 593–598 (1994).
29. M. Gu and C. J. R. Sheppard, "Three-dimensional transfer functions in 4Pi confocal microscopes," J. Opt. Soc. Am. A **11**, 1619–1627 (1994).
30. C. W. McCutchen, "Generalized aperture and the three-dimensional diffraction image," J. Opt. Soc. Am. **54**, 240–244 (1964).
31. C. W. McCutchen, "Generalized aperture and the three-dimensional diffraction image: Erratum," J. Opt. Soc. Am. A **19**, 1781 (2002).
32. B. J. Davis, W. C. Karl, A. K. Swan, M. S. Ünlü, and B. B. Goldberg, "Capabilities and limitations of pupil-plane filters for superresolution and image enhancement," Opt. Express **12**, 4150–4156 (2004).
33. P. J. Verveer, M. J. Gemkow, and T. M. Jovin, "A comparison of image restoration approaches applied to three-dimensional confocal and wide-field fluorescence microscopy," J. Microsc. **193**, 50–61 (1999).
34. M. Nagorni and S. W. Hell, "Coherent use of opposing lenses for axial resolution increase. II. Power and limitation of nonlinear image restoration," J. Opt. Soc. Am. A **18**, 49–54 (2001).
35. E. H. K. Stelzer, "Contrast, resolution, pixelation, dynamic range and signal-to-noise ratio: Fundamental limits to resolution in fluorescence light microscopy," J. Microsc. **189**, 15–24 (1998).
36. M. C. Lang, J. Engelhardt, and S. W. Hell, "4Pi microscopy with linear fluorescence excitation," Opt. Lett. **32**, 259–261 (2007).
37. I. J. Cox and C. J. R. Sheppard, "Information capacity and resolution in an optical system," J. Opt. Soc. Am. A **3**, 1152–1158 (1986).
38. M. Dogan, B. B. Goldberg, A. K. Swan, and M. S. Ünlü, "4Pi spectral self-interference fluorescence microscopy," presented at OSA Frontiers in Optics 2006/Laser Science XXII, Rochester, New York, October 8–12, 2006.
39. A. Bilenca, A. Ozcan, B. Bouma, and G. Tearney, "Fluorescence coherence tomography," Opt. Express **14**, 7134–7143 (2006).
40. A. Bilenca, T. Lasser, A. Ozcan, R. A. Leitgeb, B. E. Bouma, and G. J. Tearney, "Image formation in fluorescence coherence-gated imaging through scattering media," Opt. Express **15**, 2810–2821 (2007).
41. S. Ram, E. S. Ward, and R. J. Ober, "Beyond Rayleigh's criterion: A resolution measure with application to single-molecule microscopy," Proc. Natl. Acad. Sci. U.S.A. **103**, 4457–4462 (2006).
42. M. Schrader, K. Bahlmann, G. Giese, and S. W. Hell, "4Pi-confocal imaging in fixed biological specimens," Biophys. J. **75**, 1659–1668 (1998).
43. A. Egner, M. Schrader, and S. W. Hell, "Refractive index mismatch induced intensity and phase variations in fluorescence confocal, multiphoton and 4Pi-microscopy," Opt. Commun. **153**, 211–217 (1998).
44. D. Baddeley, C. Carl, and C. Cremer, "4Pi microscopy deconvolution with a variable point-spread function," Appl. Opt. **45**, 7056–7064 (2006).